An Investigation into Models of Cuprate Superconductivity

Mathi Raja

Honors Thesis carried out under the supervision of:
Prof. Joel Moore

University of California at Berkeley
2024

Honors thesis carried out for the degree title:

Bachelor of Arts in Physics with Honors

University of California Berkeley

Thesis written by

Mathi Raja

Berkeley, CA

Date of submission: May 10, 2024

Acknowledgements

First and foremost, I wish to give thanks to my advisor, Professor Joel Moore, whose knowledge, suggestions, and encouragement helped me carry out this thesis. It has been an honor to be advised and he has been inspirational to my journey in physics. Furthermore, I would like to acknowledge and thank Bartholomew Andrews, whose role in mentoring me last summer was indispensable and helped focus my interest in condensed matter. In addition, Adrian van Kan's guidance throughout my undergraduate years has greatly influenced me as a researcher and I would like to give my thanks to him. Finally, I would like to thank my family, Amma, Appa, and Kaviya whose continued love and encouragement have been the foundation of my passion for all my pursuits.

Contents

Acknowledgements . . . . . **i**

1 Introduction **1**

2 Models for Superconductivity **3**
2.1 The Hubbard Hamiltonian 3
2.1.1 Symmetries 4
2.2 t-J Model 6
2.3 Attractive-U 8
2.4 Heisenberg Model 9
2.5 Holstein-Primakoff Transformation 11
2.6 BCS Theory 12
2.6.1 BCS ground state 13
2.6.2 Correlation Decay 14
2.7 Meissner Effect 15
2.7.1 London Equations 15

3 MPS and DMRG **17**
3.1 Matrix Product States (MPS) 17
3.1.1 Correlation functions in MPS 18
3.2 Density Matrix Renormalization Group (DMRG) Algorithms 19
3.3 TenPy Example 21

4 Computational Schemes, Numerics, and Future Directions **24**
4.1 1D Hubbard Chain Properties 24
4.1.1 Superconducting Phase in Attractive-U 24
4.2 Mean-field Theoretic Approach 28
4.3 MPS+MF Algorithm 30
4.4 Conclusion and Future Outlook 31

1 Introduction

At the frontier of theoretical physics lies the quest to understand the collective behavior of interacting electrons and the emergent phenomena it gives rise to. This thesis embarks on a journey through understanding how electron correlations and magnetic interactions interweave to reveal the secrets of superconductivity. Specifically, cuprate materials, copper-oxide compounds have long been studied as they exhibit superconductivity at high temperatures. Their intricate arrangements of atoms give rise to a rich variety of quantum behaviors, including charge-density waves, spin fluctuations, and intriguing electronic correlations. The complex nature of cuprate materials offers an excellent opportunity for scientific exploration, and uncovering their mysteries could lead to groundbreaking technological advancements. While numerous approaches have been research to explain cuprate superconductivity, a recurring and promising framework is the Hubbard model. This model serves as a cornerstone for examining the rich phenomena exhibited by electrons in crystalline lattices, particularly their magnetic properties and the transitions into various phases, including superconductivity. While it may be simple, its ability to describe a vast array of phenomena, from ferromagnetism to high-temperature superconductivity, is unparalleled and its extensions may prove useful to potentially understanding the theory of high-temperature superconductivity.

This thesis begins by delving into the fundamentals of the Hubbard model, providing a thorough overview of its applications and limitations, and setting the stage for its extension into the complex domain of superconductivity. We then explore the limits of the Hubbard model and discuss other lattice models such as the Heisenberg model, t-J model, and attractive Hubbard model. We look at various attributes and phases of these models in hopes of getting a background to investigate superconducting phases. Understanding the theory behind superconducting phases is impossible without an introduction to BCS (Bardeen–Cooper–Schrieffer) theory, the original microscopic model of superconductivity, and we also provide a brief introduction to the subject.

The complexity of quantum many-body systems demands powerful computational methods. The thesis presents the Matrix Product States (MPS) and the Density Matrix Renormalization Group (DMRG) as tools that have significantly advanced our capability to analyze such systems. With these methods, we explore the nuanced

ground and excited state behaviors of electrons in the Hubbard model, specifically the one-dimensional Hubbard chain, and discuss how it can be used to research possible models of cuprate systems. Specifically, we explore the one-dimensional Hubbard chain using the tensor network method TenPy and monitor superconducting order parameters as well as ground state energies.

The mean-field theoretic approach serves as a foundational approximation technique that simplifies the interactions within many-body systems. By considering the effect of all other electrons as an average field, this approach allows for the derivation of tractable equations and insights into the cooperative phenomena that characterize superconductivity. The thesis ends in the discussion of a hybrid algorithm introduced by [5] that combines MPS with mean-field theory as a means to numerically understand and model more complicated cuprate systems.

The pursuit of a deeper understanding of superconductivity within the framework of the Hubbard model is both a return to foundational principles and a step into new territories of quantum physics. The review of the theory behind various lattice models, superconductivity, and the computational methods of tensor networks in this thesis not only sheds light on the intrinsic properties of low-dimensional systems but also sets the stage for future explorations into the uncharted terrains of high-temperature superconductivity.

2 Models for Superconductivity

The Hubbard model is a simple yet profoundly impactful theoretical model in condensed matter physics, especially in the study of strongly correlated materials. Originally proposed to describe electrons in magnetic and transition metal oxides, the model captures the essential physics of electron-electron interactions in a lattice and has been extensively used to explore phenomena such as magnetism, metal-insulator transitions, and superconductivity.

2.1 The Hubbard Hamiltonian

The Hubbard model focuses on the minimal ingredients necessary to explore electron correlation effects in a crystalline solid. The primary assumption is a lattice of atoms, each with a single energy level available for occupation by fermions (or bosons in some cases). The model is defined by the Hamiltonian [2, 16, 21]:

$$\hat{H} = -t \sum_{\langle i,j\rangle,\sigma} (c^{\dagger}_{i\sigma} c_{j\sigma} + c^{\dagger}_{j\sigma} c_{i\sigma}) + U \sum_{i} n_{i\uparrow} n_{i\downarrow} - \mu \sum_{i,\sigma} n_{i\sigma} \tag{1}$$

- Here, $c^{\dagger}_{i\sigma}$ and $c_{i\sigma}$ are the creation and annihilation operators for an electron with spin σ at lattice site i, and $n_{i\sigma} = c^{\dagger}_{i\sigma} c_{i\sigma}$ is the number operator that counts the electrons at site i with spin σ.

- The sum $\langle i, j\rangle$ is over nearest-neighbor pairs of sites, which restricts the movement of electrons to adjacent lattice sites.

- The first term in the Hamiltonian represents the kinetic energy of electrons hopping between adjacent lattice sites, with t being the hopping amplitude. This term tends to delocalize the electrons, spreading them evenly across the lattice, which favors a metallic state.

- The second term is the on-site Coulomb repulsion where U is the energy cost of double occupancy. This term competes with the kinetic energy term by penalizing configurations where two electrons occupy the same site.

- The third term $-\mu \sum_{i,\sigma} n_{i\sigma}$ includes the chemical potential μ, where ($n_{i\sigma} = c^{\dagger}_{i\sigma} c_{i\sigma}$ is the number operator for electrons with spin σ at site i. This term

effectively adjusts the total energy of the system based on the electron number and is essential for maintaining the desired electron concentration in the material. By tuning μ, one can control the filling level of the lattice, which is crucial for exploring different physical phenomena such as doping-induced superconductivity or transitions from metallic to insulating phases.

While the majority of this thesis will discuss the one-dimensional version of the Hubbard model, the model is more generally visualized in two dimensions as seen in the following figure:

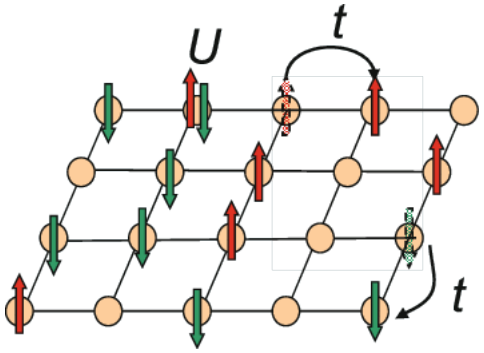

Figure 1: A visualization of spin 1/2 fermions hopping in the Hubbard model on a 2D lattice [7].

2.1.1 Symmetries

Observing the Hamiltonian, we can note that we have a continuous global U(2) symmetry which can be broken into $U(2) = U(1) \times SU(2)$, with the U(1) symmetry revealing a global charge conservation. This symmetry can be represented with our creation and annihilation operators as such:

$$c_{i\sigma}^{\dagger} \to e^{i\alpha} c_{i\sigma}^{\dagger},$$
$$c_{i\sigma} \to e^{-i\alpha} c_{i\sigma}.$$

Furthermore, the SU(2) symmetry shows that we have spin symmetry and thus, we can have good quantum numbers: $\hat{S}^z$ and $\hat{S}^2$. We have the following operators that generate the spin symmetry of the Hubbard model [2, 16]:

$$S^+ = \sum_i c^\dagger_{i\uparrow} c_{i\downarrow}, \quad S^- = (S^+)^\dagger$$
$$S^z = \frac{1}{2} \sum_i (c^\dagger_{i\uparrow} c_{i\uparrow} - c^\dagger_{i\downarrow} c_{i\downarrow})$$

The particle-hole symmetry is also a critical element of the Hubbard model, specifically at half-filling, where it profoundly influences the system's physical properties. In a bipartite lattice, particle-hole symmetry can be described by a transformation that exchanges particles and holes while flipping the spin (a hole can be thought of as the lack of a particle in a sea of particles as per its name, hole). Mathematically, this transformation can be expressed as $c_{i\sigma} \to (-1)^i c^\dagger_{i\sigma}$, where i indexes lattice sites and σ denotes spin. Here, $(-1)^i$ takes opposite signs on the two sublattices.

In the presence of this symmetry, the Hubbard Hamiltonian at half-filling can be shown to be invariant under the particle-hole transformation. This invariance leads to several crucial consequences, including the symmetric distribution of the electron occupation number at half-filling. As a result, for every electron added to the system, a corresponding hole can be thought of as being removed, keeping the system at a net zero change in particle number from half-filling.

In addition, this symmetry impacts the magnetic properties of the system. At half-filling, under strong coupling conditions ($U \gg t$), the Hubbard model reduces to an antiferromagnetic Heisenberg model. This reduction is also a manifestation of particle-hole symmetry, as the effective model describes spins that result from an equal mixture of electrons and holes, emphasizing the model's ability to capture essential magnetic interactions from purely electronic origins [3, 19].

Overall, the Hubbard model, despite its simplicity, leads to rich and complex behavior. The competition between the kinetic energy and the potential energy gives rise to a variety of phases depending on the relative strengths of t and U, the electron density, and the lattice structure. For small U/t, the system behaves as a metal with itinerant electrons. As U/t increases, the system can undergo a transition to an insulating state, often accompanied by magnetic ordering. The nature of this ordering (e.g., ferromagnetic, antiferromagnetic) depends on the lattice geometry and dimensionality as well as the electron concentration. In the 2D lattice case, it has been proven that the ground state of the Hubbard model has anti-ferromagnetic order at

any U (mott-insulator) due to super-exchange processes [20]. However, when doped, the physics of the ground state changes, revealing phases of spin density waves, charge density waves, stripes, and superconductivity [10].

Extensions of the model often include terms for longer-range hopping or interactions, additional orbitals per site, coupling to other degrees of freedom like lattice vibrations, as well as the addition of pairing terms in the Hamiltonian. These extensions serve uses to study different emergent properties in a variety of condensed matter systems such as cuprates, organic conductors, twisted bilayer graphene, transition metals, ultracold atomic gases, and more.

2.2 t-J Model

The Hubbard model's large U/t limit's low-energy excitations at half filling are governed by an effective Hamiltonian given the name the t-J Model. To derive this model, as motivated by [3], we can choose a zeroth-order Hamiltonian as

$$\mathcal{U} = U \sum_i n_{i\uparrow} n_{i\downarrow} \tag{2}$$

with eigenstates of Fock states of the form: $|n_{1\uparrow}, n_{1\downarrow}, n_{2\uparrow} \cdots \rangle$. We note that we can split our Fock space into subspaces where $n_{i\uparrow} + n_{i\downarrow} \leq 1$ or when $n_{i\uparrow} + n_{i\downarrow} = 2$. Additionally, we treat our hopping term as a perturbation of coupling the "≤ 1" subspace to the "$= 2$" subspace by hopping electrons from/to doubly occupied sites:

$$T = -\sum_{i,j,\sigma} t c^\dagger_{i\sigma} c_{j\sigma} \tag{3}$$

and we can rewrite our Hamiltonian to be partitioned as such:

$$\mathcal{H} = \begin{pmatrix} P_{\leq 1}(T + \mathcal{U})P_{\leq 1} & P_{\leq 1} T P_{=2} \\ P_{=2} T P_{\leq 1} & P_{=2}(T + \mathcal{U})P_{=2} \end{pmatrix} \tag{4}$$

We can consequently use projections onto the different subspaces and rearrange this via projecting the resolvent operator $((E - H)^{-1})$ onto the "≤ 1" subspace to get a condition such that our eigenenergies of our Hamiltonian are given by the roots of

$$\det |E_n - H^{\text{eff}}(E_n)| = 0. \tag{5}$$

H^{eff} can now be reduced in the zeroth order in E/U and second order in t/U to

$$H^{\text{eff}} \to P_{\leq 1}(T - \frac{1}{U}\sum_{i,j,k,\sigma,\sigma'} t^2 c^\dagger_{i\sigma} c_{j\sigma} n_{j\uparrow} n_{j\downarrow} c^\dagger_{j\sigma'} c_{k\sigma'}) P_{\leq 1}(1 + \mathcal{O}(E/U) + \mathcal{O}(t/U)) \quad (6)$$

where $P_{\leq 1}$ is the projective operator onto the subspace of eigenstates of $\mathcal{U}$ with $n_{i\uparrow} + n_{i\downarrow} \leq 1$ and T is the hopping term treated as a perturbation. Ignoring $\mathcal{O}(E/U)$ and $\mathcal{O}(t/U))$ terms, we can rewrite

$$P_{\leq 1}(T - \frac{1}{U}\sum_{i,j,k,\sigma,\sigma'} t^2 c^\dagger_{i\sigma} c_{j\sigma} n_{j\uparrow} n_{j\downarrow} c^\dagger_{j\sigma'} c_{k\sigma'}) P_{\leq 1} = H^{t-J} \quad (7)$$

Rearranging this using fermion operators, we can see that

$$H^{t-J} = P_{\leq 1}(T + H^{QHM} + \mathcal{J}')P_{\leq 1} \quad (8)$$

where H^{QHM} is the quantum Heisenberg model with

$$H^{QHM} = \frac{1}{2}\sum_{i,j} J(\mathbf{S_i} \cdot \mathbf{S_j} - \frac{n_i n_j}{4}) \quad (9)$$

$$\mathcal{J}' = -\frac{1}{2U}\sum_{i,j,k}^{i\neq k} t^2 \left(\sum_\sigma (c^\dagger_{i\sigma} c_{k\sigma} n_j) - c^\dagger_i \vec{\sigma} c_k \cdot c^\dagger_j \vec{\sigma} c_j\right) \quad (10)$$

and we can omit the $\mathcal{J}'$ term as its effect is small in comparison to the t hopping as per the literature [3]. Defining our superexchange coupling constant as

$$J = \frac{4t^2}{U}, \quad (11)$$

we are left with our effective Hamiltonian which we refer to as the t-J model (including only nearest neighbor hopping):

$$H^{t-J} = -t\sum_{\langle i,j\rangle,\sigma}\left(\hat{c}^\dagger_{i\sigma}\hat{c}_{j\sigma} + \hat{c}^\dagger_{j\sigma}\hat{c}_{i\sigma}\right) + J\sum_{\langle i,j\rangle}\left(\mathbf{S}_i \cdot \mathbf{S}_j - \frac{n_i n_j}{4}\right) \quad (12)$$

Specific details of the effective reduction using the projections to the separate Fock subspaces have been omitted/summarized here but an expansive derivation is given in [3].

At half filling, the t-J model reduces to the quantum Heisenberg antiferromagnetic which we will discuss in a few sections, but away from half filling, we can describe the t-J model as representing a system called the doped antiferromagnet" [3]. The t-J model also has possibilities for high-temperature superconductivity when in a spin-liquid phase, aided by dilute polarons, quasiparticles that are coupled to low-energy spin fluctuations, and in which long-range spin order disappears although at small length scales, antiferromagnetic correlations exist.

2.3 Attractive-U

If we allow $U < 0$, we have a Hubbard model that hosts attractive interactions between electrons, meaning they can obtain negative pair-binding energy by collectively polarizing a degree of freedom. Certain methods of polarization to achieve this attraction between electrons include phonon (quantization of lattice vibration modes) interaction (see BCS theory), plasmons (quantization of plasma oscillations), and spin fluctuations.

Note that we can also transform our attractive U model to a positive-U model by using the following Bogoliubov transformation [6, 14]:

$$\begin{aligned} c_{i\uparrow} &\to c_{i\uparrow} \\ c_{i\downarrow} &\to c^{\dagger}_{i\downarrow}. \end{aligned} \tag{13}$$

This transformation also maps the charge operators of our original model into pseudo-spin operators of our new positive-U model: $\frac{1}{2}(n_i - 1) \Leftrightarrow S^z_i$. Therefore, we can see the duality between charge density waves in the negative-U model and z-spin density waves in the positive-U model. Thus, we can write our pseudo-spin operators S^x and S^y as corresponding to pairing operators:

$$\begin{aligned} \frac{1}{2}(c^{\dagger}_{i\uparrow}c^{\dagger}_{i\downarrow} + c_{i\downarrow}c_{i\uparrow}) &= S^x_i \\ \frac{1}{2i}(c^{\dagger}_{i\uparrow}c^{\dagger}_{i\downarrow} - c_{i\downarrow}c_{i\uparrow}) &= S^y_i \end{aligned} \tag{14}$$

Thus, treating the ordering of pseudo-spins as such, we can recognize this as

superconductivity in the negative-U model with the magnitude of ordered moments $\langle S_i^+ \rangle$ as the BCS order parameter Δ.

The physical properties of the attractive-U Hubbard model depend significantly on $|U|/t$ as well as the average occupation $\langle n \rangle$. While at equal to or larger dimensions than three at half filling have a critical temperature and phase transition between a disordered phase and a phase with charge-density waves as well as superconductivity, for two-dimensional systems the critical temperature at half filling is 0 [17].

Another interesting property of the attractive U Hubbard model is that it forms a model of superconductivity due to the attractive interactions between electrons, modeling the formation of bound pairs of electrons, known as Cooper Pairs. These pairs can move through the lattice without resistance, a phenomenon aiding certain types of superconductivity. Furthermore, the model also hosts phases of charge density waves and bi-polaronic states. Attractive interactions can also lead to instabilities towards the formation of charge density waves, where electrons tend to cluster, leading to a periodic modulation in the electron density across the lattice. Two electrons can form a bi-polaron, a bound state of two electrons localized on the same site, which can be more stable due to the attractive interaction. This can lead to different ground state properties compared to the repulsive case. Also, the system can exhibit phase separation, where it spontaneously divides into regions with high and low electron densities. Finally, even with negative U, the model can display a Mott insulator transition, although under different conditions from the positive U case. Here, the transition can involve the formation of an insulating state due to the localization of electron pairs rather than individual electrons [6, 17].

2.4 Heisenberg Model

The Heisenberg model, as mentioned earlier, can be derived as an effective model from the Hubbard model in the limit of strong on-site electron-electron interaction relative to the kinetic energy term. Seeing our derivation of the t-J model, note that at half filling we have $n_i = 1$, so in this case, low energy hopping cannot exist and we are in a Mott insulator phase meaning that the only term that survives the projection to the subspace in which $n_{i\uparrow} + n_{i\downarrow} \leq 1$ is the H^{QHM} term from above, or the Heisenberg model Eq. 9 with exchange energy interaction as given before (after using $n_i = 1$ and shifting zero-energy):

$$H_{\mathrm{QHM}} = J \sum_{\langle i,j \rangle} \mathbf{S}_i \cdot \mathbf{S}_j. \tag{15}$$

In other words, in the strong coupling limit ($U \gg t$), the Hubbard model simplifies due to the energy cost of doubly occupied states becoming extremely large where we needed to consider the second-order perturbation theory, where the kinetic term acts as a perturbation to the interaction term. Under this condition, the relevant configuration space includes states where each site is either singly occupied or empty. Double occupancy is energetically unfavorable and thus excluded from low-energy states. The factor of four in the exchange energy interaction (Eq. 11) arises from the two possible hopping processes (forward and backward) between nearest neighbor sites i and j, each contributing an energy change of $\frac{t^2}{U}$.

The spin operators $\mathbf{S}_i$ in this case are related to the fermionic operators by:

$$S_i^+ = c_{i\uparrow}^\dagger c_{i\downarrow}, \quad S_i^- = c_{i\downarrow}^\dagger c_{i\uparrow}, \quad S_i^z = \frac{1}{2}(n_{i\uparrow} - n_{i\downarrow}), \tag{16}$$

which are the standard expressions for the spin-1/2 raising, lowering, and z-component operators in terms of fermionic creation and annihilation operators.

The resultant effective Hamiltonian, the Heisenberg model, encapsulates the spin-spin interaction dynamics without explicit reference to the electron's charge degree of freedom, focusing solely on their spin interactions. This model is crucial in the study of magnetic insulators where the charge degrees of freedom are frozen out, but spin degrees of freedom remain dynamically significant.

The Heisenberg model hosts a variety of phases and interesting behaviors. At high temperatures, thermal fluctuations are strong such that spins lack a certain order, but below a critical temperature, spins may align. This critical temperature is called the Curie temperature or the Neel temperature depending on whether we are discussing ferromagnets or antiferromagnetic respectively. In the low temperature regime, we can note from the Hamiltonian that since we have nearest neighbor spin-exchange interaction, it is simply the sign of J which determines the magnetic order [16]:

- Ferromagnetic order: If $J > 0$, the spins prefer to align parallel to each other. This alignment minimizes the energy of the system, leading to a macroscopic magnetic moment.

- Antiferromagnetic order: If $J < 0$, the spins prefer to align antiparallel to each

other, resulting in adjacent spins pointing in opposite directions. This leads to a cancellation of the overall magnetic moment, although local moments still exist.

2.5 Holstein-Primakoff Transformation

While discussing these lattice models, it is important to note the different types of tools and theories associated with them. To start, the Holstein-Primakoff transformation is a method to express spin operators in terms of bosonic creation ($a_i^\dagger$) and annihilation (a_i) operators, helping the study of spin systems using techniques from quantum field theory. This transformation is particularly useful for systems with a large total spin S and to understand spin waves/collective magnetic excitations, as it allows for an approximate linearization of the spin operators, with the mapping given by [16]:

$$S_i^+ = \sqrt{2S - a_i^\dagger a_i}\, a_i, \qquad S_i^- = a_i^\dagger \sqrt{2S - a_i^\dagger a_i}, \tag{17}$$

$$\text{and} \quad S_i^z = S - a_i^\dagger a_i \tag{18}$$

where S_i^+ and S_i^- are the spin raising and lowering operators, respectively. This approximation becomes exact in the limit of large S, and the non-commuting aspects of the spin operators are preserved [3].

The square root in the transformation introduces a non-linear term which complicates the algebra but can be simplified under the assumption of low occupation numbers of the bosons, $\langle a_i^\dagger a_i \rangle \ll 2S$, which is typically valid near the ground state of large spin systems. Under this assumption, the transformations for S_i^+ and S_i^- can be approximated as:

$$S_i^+ \approx \sqrt{2S} a_i \tag{19}$$

$$S_i^- \approx \sqrt{2S} a_i^\dagger \tag{20}$$

This linear approximation is valid in the limit of small fluctuations around the ordered state and is particularly useful in deriving the spin-wave Hamiltonian for low-energy excitations in magnetically ordered systems.

Following the above transformation, spin-wave theory is an effective approach to describe the collective excitations in a magnetically ordered system. For a ferromagnet, these excitations (spin waves), correspond to small deviations from the uniform spin alignment. The basic premise of spin-wave theory in the context of the Heisenberg model involves linearizing the Holstein-Primakoff transformation to obtain an effective Hamiltonian that describes these low-energy excitations:

$$H_{\text{sw}} = \sum_k \omega_k a_k^\dagger a_k \tag{21}$$

where $a_k^\dagger$ and a_k are the Fourier transforms of the bosonic operators, and ω_k represents the dispersion relation of the magnons, which generally depends on the wavevector k and the exchange interaction J. In the simplest cases, ω_k is proportional to k^2, reflecting the quadratic nature of these excitations in a ferromagnet [16].

2.6 BCS Theory

BCS (Bardeen-Cooper-Schrieffer) theory is the foundational theory for understanding conventional superconductivity, proposed by John Bardeen, Leon Cooper, and Robert Schrieffer in 1957. This theory explains how electron pairs, known as Cooper pairs, can form through electron-phonon interactions and thereby produce superconductivity. The theory starts with the concept of Cooper pairs, two electrons with opposite spins and momenta pair up due to an attractive interaction mediated by phonons (quantized lattice vibrations). The Hamiltonian describing this electron-phonon interaction in a superconductor is given by [4]:

$$H = \sum_{\mathbf{k},\sigma} \epsilon_{\mathbf{k}} c_{\mathbf{k}\sigma}^\dagger c_{\mathbf{k}\sigma} - V \sum_{\mathbf{k},\mathbf{k}',\mathbf{q}} c_{\mathbf{k}+\mathbf{q},\uparrow}^\dagger c_{-\mathbf{k}-\mathbf{q},\downarrow}^\dagger c_{-\mathbf{k}',\downarrow} c_{\mathbf{k}',\uparrow} \tag{22}$$

Here, $\epsilon_{\mathbf{k}}$ is the kinetic energy of electrons with wave vector $\mathbf{k}$, $c_{\mathbf{k}\sigma}^\dagger$ and $c_{\mathbf{k}\sigma}$ are the creation and annihilation operators for an electron with spin σ, and V is the potential describing the attractive interaction (electron-phonon pairing).

The first question in BCS theory is answer the Cooper problem, where two electrons form a bound state in the presence of a constant attractive potential V. The Schrödinger equation for this two-electron system is solved by assuming a trial wave function:

$$\Psi(\mathbf{r}_1, \mathbf{r}_2) = \sum_{\mathbf{k}} g(\mathbf{k}) e^{i\mathbf{k}\cdot(\mathbf{r}_1 - \mathbf{r}_2)} \tag{23}$$

The resulting equation for our pre-factor $g(\mathbf{k})$ leads to the condition that the total energy of the pair, $2\epsilon_{\mathbf{k}} - E$, must be negative, indicating a bound state, resulting in the formation of Cooper pairs below a critical temperature T_c.

2.6.1 BCS ground state

The BCS ground state can be described as a superposition of pair states where the wave function is:

$$|\Psi_{\text{BCS}}\rangle = \prod_{\mathbf{k}} (u_{\mathbf{k}} + v_{\mathbf{k}} c^{\dagger}_{\mathbf{k}\uparrow} c^{\dagger}_{-\mathbf{k}\downarrow})|0\rangle \tag{24}$$

Where $u_{\mathbf{k}}$ and $v_{\mathbf{k}}$ are undetermined coefficients. Summarizing the steps, minimizing the energy with respect to these parameters under the constraint $u^2_{\mathbf{k}} + v^2_{\mathbf{k}} = 1$ leads to the self-consistent BCS gap equation [4, 16]:

$$\Delta_{\mathbf{k}} = -\sum_{\mathbf{k}'} V_{\mathbf{k}\mathbf{k}'} \frac{\Delta_{\mathbf{k}'}}{2E_{\mathbf{k}'}} \tanh\left(\frac{\beta E_{\mathbf{k}'}}{2}\right) \tag{25}$$

Here, $E_{\mathbf{k}} = \sqrt{(\epsilon_{\mathbf{k}} - \mu)^2 + |\Delta_{\mathbf{k}}|^2}$ is the quasiparticle energy, $\Delta_{\mathbf{k}}$ is the gap parameter, and $\beta = 1/(k_B T)$.

The specific heat of a superconductor undergoes a significant change at T_c. In the normal state, the specific heat C varies linearly with temperature, but in the superconducting state, it shows an exponential behavior due to the energy gap $\Delta(T)$ at the Fermi surface. Near T_c, the specific heat jumps discontinuously, which is a hallmark of the phase transition. BCS theory gives an expression for the specific heat below T_c as [16]:

$$C_s = C_n \cdot \exp\left(-\frac{\Delta(0)}{k_B T}\right) \tag{26}$$

where C_s is the specific heat in the superconducting state, C_n is the specific heat in the normal state, and $\Delta(0)$ is the superconducting gap at zero temperature.

The superconducting gap $\Delta(T)$ is a critical order parameter that determines many properties of a superconductor. BCS theory provides a temperature-dependent form

of the gap, which closes at T_c. At $T = 0$, the gap reaches its maximum, $\Delta(0)$, and it is given by:

$$\Delta(T) \propto k_B T_c \left(1 - \frac{T}{T_c}\right)^{\frac{1}{2}}. \tag{27}$$

2.6.2 Correlation Decay

In superconducting systems, the decay of correlations, particularly those related to the superconducting order parameter, provides important insights into the nature and robustness of the superconducting state. The decay behavior of these correlations depends primarily on whether the superconductor is in its normal or superconducting state, and on the fundamental characteristics of the superconducting phase itself—such as whether it's a conventional (s-wave) or unconventional (p-wave, d-wave, etc.) superconductor.

In the superconducting state, the decay of correlations is fundamentally influenced by the presence of an energy gap, the coherence length, and the type of pairing symmetry. In conventional superconductors with a uniform gap in the excitation spectrum (s-wave), superconducting correlations, which can be associated with the Cooper pair wave function, typically exhibit exponential decay at distances beyond the coherence length, ξ. In fact, this power law behavior is true of all states which have a spectral gap above the ground state in fermionic systems with short-range interactions [8]. The correlation function $C(r)$ for such systems decays as:

$$C(r) \propto e^{-r/\xi} \tag{28}$$

This behavior is indicative of a stable superconducting phase with short-range correlations in the order parameter and is proven mathematically for all gapped systems by the Lieb-Robinson bound [8].

In high-temperature superconductors and other unconventional superconductors/-gapless systems, the presence of nodes (points on the Fermi surface where the gap vanishes) can lead to different decay behaviors. In regions close to the nodes, the superconducting gap approaches zero, leading to quasi-particle excitations that can propagate over longer distances. This results in a power-law decay of correlations at

zero temperature, typically observed as:

$$C(r) \propto \frac{1}{r^n} \tag{29}$$

where n is determined by the low-energy excitations near the "zero" points.

Above the critical temperature T_c, superconductors transition to a normal state where superconducting correlations vanish. In this state close to T_c, superconducting fluctuations can still induce transient superconducting-like correlations, which usually decay exponentially but with a correlation length that diverges as the temperature approaches T_c from above. This behavior is described by:

$$C(r) \propto e^{-r/\xi(T)} \tag{30}$$

where $\xi(T) \sim |T - T_c|^{-\nu}$, with critical exponent ν.

2.7 Meissner Effect

Another aspect of correlation decay in superconductors involves the magnetic field penetration depth, λ, which describes how magnetic fields decay exponentially inside a superconductor. This is a manifestation of the Meissner effect, where:

$$B(r) = B_0 e^{-r/\lambda}. \tag{31}$$

This is named the "London penetration depth" where λ can be recognized as [16]:

$$\lambda = \sqrt{\frac{m}{\mu_0 n q^2}} \tag{32}$$

where m is mass, q is charge, and n is number density. This formula can be derived via the London equations which we will now discuss.

2.7.1 London Equations

The London equations are based on a simple modification of the classical electrodynamics suited to the behavior of superconductors and describe how superconductors expel electromagnetic fields. The two London equations can be written as [16, 3]:

$$\nabla \times \mathbf{J} = -\frac{1}{\lambda^2}\mathbf{B} \tag{33}$$

This equation suggests that the curl of the supercurrent density $\mathbf{J}$ is proportional to the negative of the magnetic field $\mathbf{B}$. Here, λ is the London penetration depth, which characterizes how deeply magnetic fields can penetrate into a superconductor.

$$\frac{\partial \mathbf{J}}{\partial t} = \frac{n_s e^2}{m}\mathbf{E} \tag{34}$$

This states that the rate of change of the supercurrent is proportional to the electric field $\mathbf{E}$. This equation is derived under the assumption that the superconducting electrons (density n_s) behave as if they have no mass in response to electric fields due to their paired state in the superconductor.

To derive the Meissner effect, we begin with the first London equation and apply a curl both sides and using Maxwell's equations, we get:

$$\nabla \times (\nabla \times \mathbf{J}) = -\frac{1}{\lambda^2}\nabla \times \mathbf{B} \tag{35}$$

$$\nabla(\nabla \cdot \mathbf{J}) - \nabla^2 \mathbf{J} = -\frac{\mu_0}{\lambda^2}\mathbf{J} \tag{36}$$

Assuming $\nabla \cdot \mathbf{J} = 0$ (charge conservation), we simplify this to:

$$\nabla^2 \mathbf{J} = \frac{\mu_0}{\lambda^2}\mathbf{J} \tag{37}$$

Using Maxwell's equations again and substituting, we derive a similar equation for $\mathbf{B}$:

$$\nabla^2 \mathbf{B} = \frac{1}{\lambda^2}\mathbf{B} \tag{38}$$

This is the key differential equation describing the exponential decay of the magnetic field in a superconductor and we can solve this to find (given the boundary condition that $\mathbf{B}$ approaches the external field $\mathbf{B}_0$ at the surface):

$$\mathbf{B}(r) = \mathbf{B}_0 e^{-r/\lambda} \tag{39}$$

where r is the distance from the surface of the superconductor.

3 MPS and DMRG

Quantum many-body systems are extremely difficult to solve due to the exponential growth of the Hilbert space with the number of particles. Traditional methods like exact diagonalization become impossibly intensive even for somewhat small systems. Thus, this has spurred the development of alternative computational approaches. Matrix Product States (MPS) and tensor network methods stand out for their efficiency and accuracy in one-dimensional systems. A tensor network represents a quantum state as a network of interconnected tensors, where each tensor's indices represent physical or virtual degrees of freedom. The primary advantage of tensor networks is their ability to represent entangled quantum states efficiently. While a general quantum state of N particles may require storing 2^N complex coefficients, tensor networks can often approximate these states with far fewer parameters by exploiting the structure of quantum entanglement. Furthermore, allowing for more dimensions and truncating tensor dimension lengths allows for efficient and better approximated numerical optimizations [9, 12].

In the context of the Hubbard model, which is pivotal for understanding phenomena like high-temperature superconductivity, MPS and DMRG have enabled the calculation of ground state properties and dynamics under various conditions. The flexibility of MPS to handle different interaction terms and lattice geometries makes it particularly suitable for studying complex behaviors in the Hubbard model.

3.1 Matrix Product States (MPS)

A MPS is a specific type of tensor network where the quantum state is decomposed into a chain of tensors, each linked by a matrix product. The standard form of an MPS for a system of N particles is given by:

$$|\psi\rangle = \sum_{\{i_k\}} \mathrm{Tr}(A^{[1]i_1} A^{[2]i_2} \dots A^{[N]i_N}) |i_1 i_2 \dots i_N\rangle$$

where $A^{[k]i_k}$ are matrices associated with the k-th site and i_k are the physical indices corresponding to the quantum state at each site (e.g., spin up or down). The product of matrices across the chain captures the entanglement and correlations between different parts of the system.

One of the key strengths of MPS is the control over the bond dimension χ, the di-

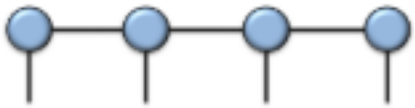

Figure 2: Matrix product state tensor network diagram with open boundary conditions for 4 sites [12].

mension of the matrices connecting the tensors. This dimension dictates the amount of entanglement that can be captured between different parts of the system. In practice, χ provides a tunable parameter that balances accuracy against computational cost. For gapped one-dimensional systems, MPS with moderate χ often yield highly accurate results.

3.1.1 Correlation functions in MPS

We can define correlation functions in MPS, but since we are dealing with a finite number of tensors and exponential decay with separation distance, the correlation length of MPS is always finite and thus we cannot reproduce scale-invariant systems. Fortunately, we do not deal with such critical systems here and are instead interested in ground states in which we can find correlation functions.

For example, given an infinite MPS defined for some tensor A, we can define the two-body correlator

$$C(r) = \langle O_i O'_{i+r} \rangle - \langle O_i \rangle \langle O'_{i+r} \rangle \tag{40}$$

which can be diagrammatically represented as seen in Fig. 3.

To compute such correlation functions, we start by transforming the MPS into a mixed canonical form where the MPS is left-normalized up to site i and right-normalized from site j. This transformation places the system in an optimal form for contraction, as it ensures that the identity relations for the matrices hold outside the interval [i, j], simplifying the contractions required to compute the expectation value.

We then proceed by expressing the correlation function in terms of a series of tensor contractions, involving the tensors representing the MPS at sites i through j and their conjugates, connected by the corresponding transfer matrices. Transfer matrices are central to the efficient calculation of correlation functions in MPS, allowing us to

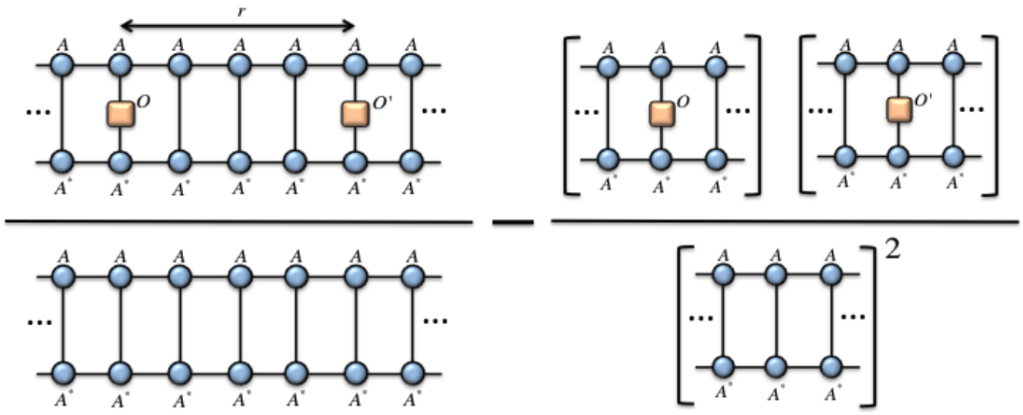

Figure 3: Diagrams for the two-body correlation function [12].

study long-range interactions without having to calculate every single interaction throughout the entire system [1].

3.2 Density Matrix Renormalization Group (DMRG) Algorithms

The Density Matrix Renormalization Group (DMRG) is a highly effective numerical algorithm used primarily for low-dimensional quantum systems, particularly one-dimensional systems and quasi-two-dimensional systems. Traditional methods struggled with quantum many-body systems due to the exponential growth of the state space with system size. DMRG, however, originally formulated for one-dimensional spin chains, overcame this problem by iteratively improving the approximation of the ground state, focusing on maintaining the most relevant states during the renormalization process [18].

The core idea of DMRG is to optimize the wave function systematically by retaining the most significant states as determined by the density matrix of a subsystem. This approach is rooted in quantum information theory, where the entanglement between subsystems plays a crucial role.

The DMRG procedure involves the following steps [18, 9]:

1. The system is divided into a block (subsystem) and an environment. Initially, the block is small, often starting with just one or two sites, and the environment includes the rest of the system.

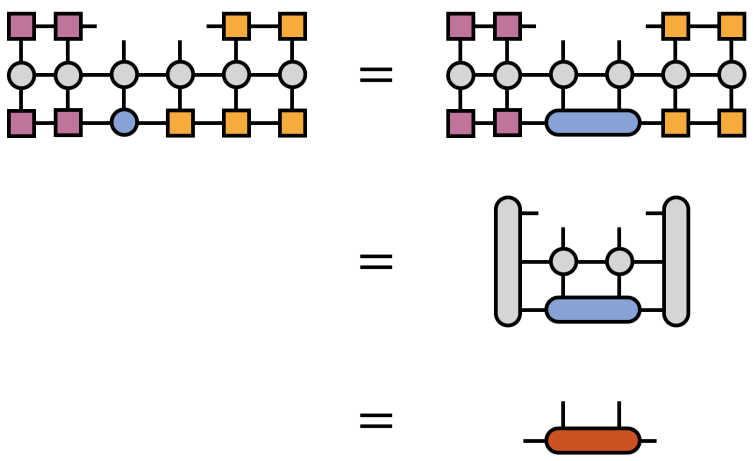

Figure 4: Diagram showing (in diagrammatic tensor notation) how the DMRG algorithm optimizes over bonds [1].

2. The state of the system is represented using Matrix Product States (MPS). Each iteration of the algorithm optimizes the MPS by focusing on one or two sites at a time.

3. For a given block, the reduced density matrix is computed by tracing out the environment's degrees of freedom. This density matrix describes all possible states of the block in the context of the entire system.

4. The density matrix is diagonalized, and its eigenvalues (which represent the probability of each state) are examined. Only the states corresponding to the largest eigenvalues are kept, effectively reducing the dimensionality of the problem but keeping the most significant contributions to the ground state.

5. The algorithm 'sweeps' through the system, alternating between optimizing the block and the environment, expanding the block by adding one site at a time from the environment, and then shrinking the environment correspondingly. After reaching the end of the chain, the sweep is reversed.

6. This sweeping is repeated until the results converge, typically indicated by the stabilization of the ground state energy or other properties of interest.

Overall, in DMRG, the Hamiltonian of the system can be expressed in terms of local terms involving only a few neighboring sites. The goal is to minimize the

expectation value of the Hamiltonian, $\langle\psi|H|\psi\rangle$, where $|\psi\rangle$ is the MPS representation of the wave function. During each step of the algorithm, the MPS is optimized locally by solving a smaller eigenvalue problem, which is computationally more feasible than solving the full system's Hamiltonian directly.

Looking at Fig. 4, we see 3 steps being taken representing the main steps taken over the algorithm. First, two tensors which share a bond index are contracted and multiplied by the Hamiltonian, H. H is also contracted with all the other MPS tensors so that it is transformed into the same basis where the bond tensor is defined [1]. After the bond tensor is optimized as such, using SVD, we factorize it and restore our MPS tensor form so that we can run the same process for the next bonds.

Physically, DMRG is effective because it exploits the area law of entanglement in one-dimensional systems, where the entanglement entropy between a block and its environment does not grow significantly with the size of the system. This allows the algorithm to maintain a manageable number of states without losing significant information about the system's ground state. DMRG has been extended many other systems, including fermions and bosons in one-dimensional and quasi-two-dimensional systems, and we seek to use it to approximate the ground state of the Hubbard model and similar models of cuprates.

3.3 TenPy Example

In this thesis, we choose to use these tensor network methods via TenPy. TenPy is particularly focused on one-dimensional systems and provides robust tools for implementing algorithms such as the Density Matrix Renormalization Group (DMRG) and various forms of tensor network state (TNS) methods, including Matrix Product States (MPS) and Projected Entangled Pair States (PEPS). TenPy supports various models like the Heisenberg model, the Hubbard model, and others, directly out of the box so we use the software to reduce coding complexity.

As there are not an abundance of resources for TenPy yet although "https://tenpy.readthedocs.io/" is fantastic, so it is useful to show an example of how to run a simple (infinite) DRMG algorithm on a 1D Hubbard chain. The following algorithm as written runs this process with suggested DMRG parameters from various trials:

Listing 1: Basic TenPy DMRG Example

```
from tenpy.models.hubbard import FermiHubbardChain
from tenpy.networks.mps import MPS
from tenpy.networks.site import SpinHalfFermionSite
from tenpy.algorithms import dmrg
from tenpy.linalg import np_conserved as npc

def run_dmrg(L, t, U, N_up, N_dn):
    # Parameters
    chi_max = 50
    model_params = {
        'L': L,
        'bc_MPS': 'infinite',  # Boundary condition
        'cons_N': 'N',      # Conservation of particle number
        't': t,             # Hopping amplitude
        'U': U,             # On-site interaction
        'verbose': 0,         # Verbosity level
        'conserve': None
    }
    eng = None
    M = FermiHubbardChain(model_params)
    site = SpinHalfFermionSite()
    prod_state = ['full', 'empty']*(M.lat.N_sites//2)
    dmrg_params = {
    'mixer': True,  # Helps to escape local minima
    'mixer_params': {
        'amplitude': 1.e-5,
        'decay': 1.2,
        'disable_after': 30
    },
    'trunc_params': {
        'svd_min': 1.e-10,
    },
    'chi_list': {0: 9, 10: 49, 20: chi_max}, #40: chi_max},
    'max_E_err': 1.e-6,
    'max_S_err': 1.e-6,
    'max_sweeps': 150,
    'verbose': 1,
    }
    psi = MPS.from_product_state(M.lat.mps_sites(),
          prod_state,bc=M.lat.bc_MPS)
    eng = dmrg.TwoSiteDMRGEngine(psi, M, dmrg_params)
    E, psi = eng.run()
    return E, psi
```

More complicated variants of this algorithm are used extensively in the results attached to this thesis and will aid future attempts to use MPS to investigate the models described in Sec. 2. Moreover, another important aspect of TenPy is to monitor the properties of these models, such as ground state, phase transitions, and dynamics. In this thesis, we concentrate on superconductivity so the natural property to observe is the superconducting order parameter as mentioned in Eq. 41 and Eq. 42

Correlation functions in TenPy can be done by calling the following on our MPS state in the case where we only have two site terms: MPS.correlation_function(). For more than two site correlators, for example in Eq. 42, we must use more clever methods such as MPS.term_correlation_function_right(); see [9] for more information.

4 Computational Schemes, Numerics, and Future Directions

4.1 1D Hubbard Chain Properties

Introducing the 1D Hubbard chain, we seek to monitor our superconducting order parameter to verify our effective Hamiltonians. Note that the attractive 1D Hubbard model can be described as a Tomonaga–Luttinger liquid (potentially superconducting) with attractive U ($U \leq 0$) as it favors the formation of Cooper pairs [10, 16].

We define the superconducting Cooper pair correlation function for s-wave superconductivity as:

$$\Delta(i,j) = \langle c^\dagger_{i,\uparrow} c^\dagger_{i,\downarrow} c_{j,\downarrow} c_{j,\uparrow} \rangle \tag{41}$$

where $\Delta(i,j)$ measures the correlation between a Cooper pair created at site i and annihilated at site j.

We define the singlet pairing (pair-field) correlation function for the 1D Fermi-Hubbard model as:

$$P^{\text{singlet}}_{ij} = \langle \Delta^\dagger_i \Delta_j \rangle \tag{42}$$

where $\Delta^\dagger_i$ is the creation operator for a singlet pair at site i, and Δ_j is the corresponding annihilation operator at site j. The singlet pair operators are defined as:

$$\Delta^\dagger_i = c^\dagger_{i\uparrow} c^\dagger_{i+1\downarrow} - c^\dagger_{i\downarrow} c^\dagger_{i+1\uparrow}$$

$$\Delta_j = c_{j+1\downarrow} c_{j\uparrow} - c_{j+1\uparrow} c_{j\downarrow}.$$

4.1.1 Superconducting Phase in Attractive-U

Using the methods discussed above in Sec. 3, specifically in the "TenPy Example", we arrive at the following singlet correlation plots for the attractive-U Hubbard chain at $L = 20$, $U = -5$, and half-filling:

We ran our DMRG algorithm with a max bond length of 50 in order to balance accuracy and computation time. Note that we actually see an exponential law correlation from the graph which is unusual as we expect power law behavior from a gapless charge excitation state as is Tomonaga–Luttinger liquids. Furthermore, as we expect s-wave superconductivity in this case, using the same parameters, we also test

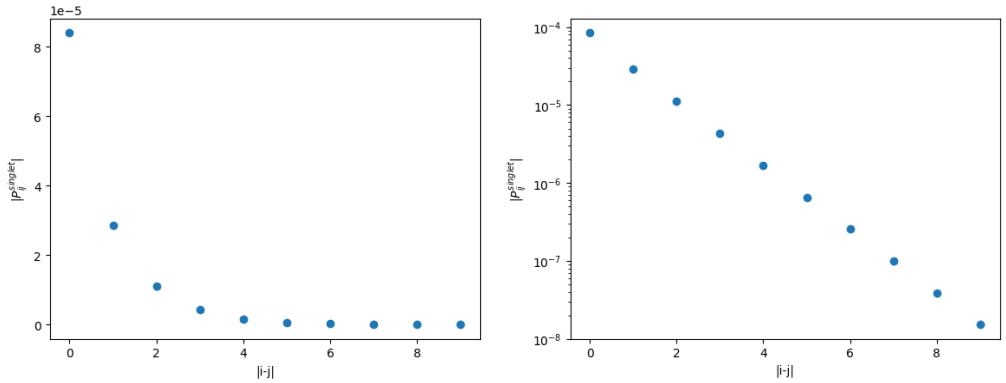

Figure 5: Left: Correlation function of superconducting pair-field order parameter P_{ij}^{singlet}. Right: y-axis log scaled to better see the exponential behavior.

the s-wave Cooper pair order parameter $\Delta(i, j)$.

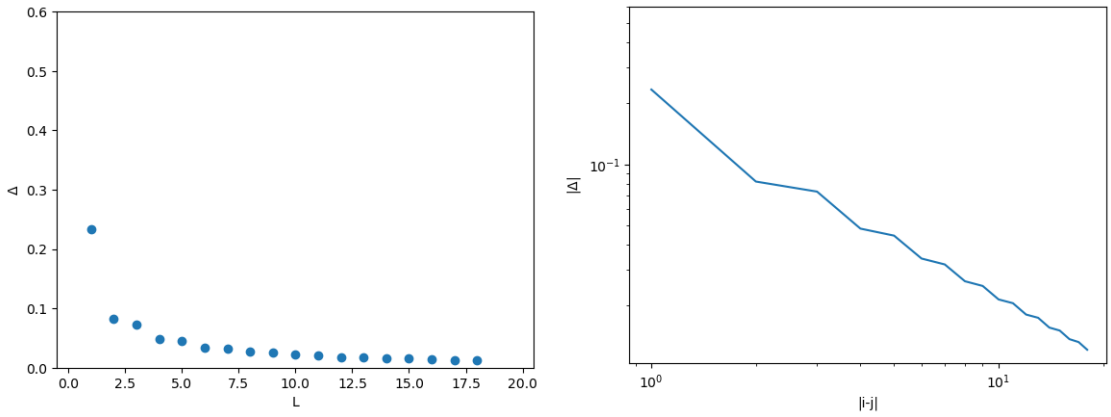

Figure 6: Left: Plotted s-wave Cooper pair correlation function as a function of distance. Right: We approximately see a power law behavior from the graph as is shown to the right.)

Fitting the profile of our correlation function, we see that we get a critical exponent of about -1.72 with a reasonable fit ($\chi^2 \approx 0.133$). Thus, we conclude that our DMRG method has shown us that the attractive-U, 1D Hubbard model shows signs of superconductivity in its Tomonaga–Luttinger liquid phase as seen by the behavior of the s-wave correlation function with respect to distance.

For our 1D Hubbard model, the exact energies are known from the Bethe ansatz method [11, 15], so we can attempt to compare our energies. To do so, we take the same chain size $L = 20$, hopping strength $t = 1$, and filling, but change U. As per

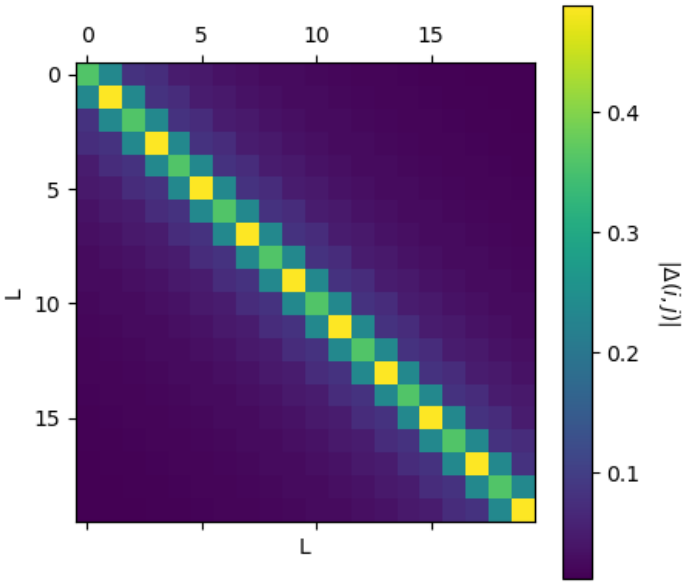

Figure 7: Displayed matrix of the superconducting pair correlation function for 1D Hubbard model via DMRG at half-filling.

[13], they approximate using the ground state using the Bethe ansatz in the small-U limit with a perturbative expansion as:

$$\frac{-4}{\pi} + \frac{1}{4}\frac{U}{t} - 0.0169961\frac{U^2}{t^2}. \tag{43}$$

Thus, we plot our results compared to the theoretical prediction in the $U \ll t$ limit as described by [13] in Fig. 8.

For completeness, we also include the following graph showing the convergence of the DMRG algorithm to the ground state energy as a function of bond dimension for $U = 0.5$ with other parameters the same as before:

We note that at larger U, we notice that our approximation diverges from the theory which is expected. More surprisingly, at very small U, we also see slight divergence which may be due to numerical issues.

For numerical convenience, we also give an example (Fig. 9) of how the ground state energy as approximated by our DMRG algorithm varies with the maximum bond dimension we set when we do our computation. We see our scheme is quite good for the 1D Hubbard model and improvements are very small even starting from a relatively small bond dimension.

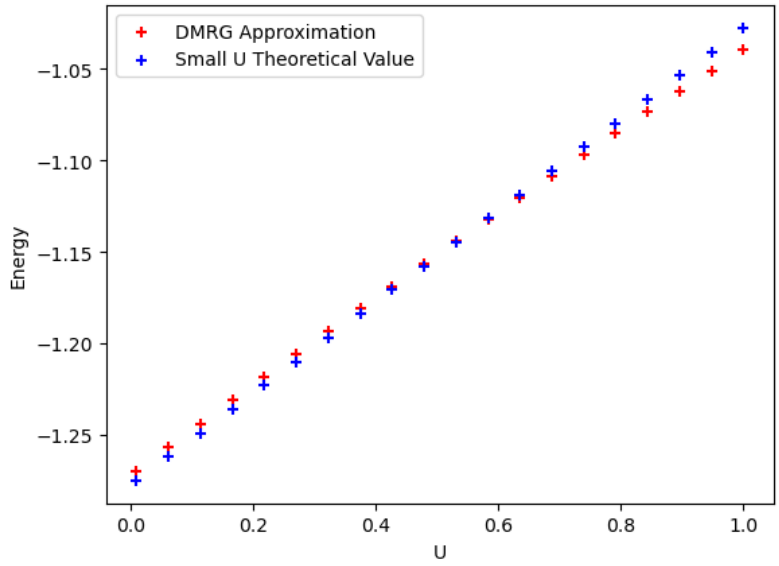

Figure 8: Scatter plot of the theoretical energy value for the 1D Fermi Hubbard Chain as according to [13] and the DMRG approximation for it at $U \ll t$.

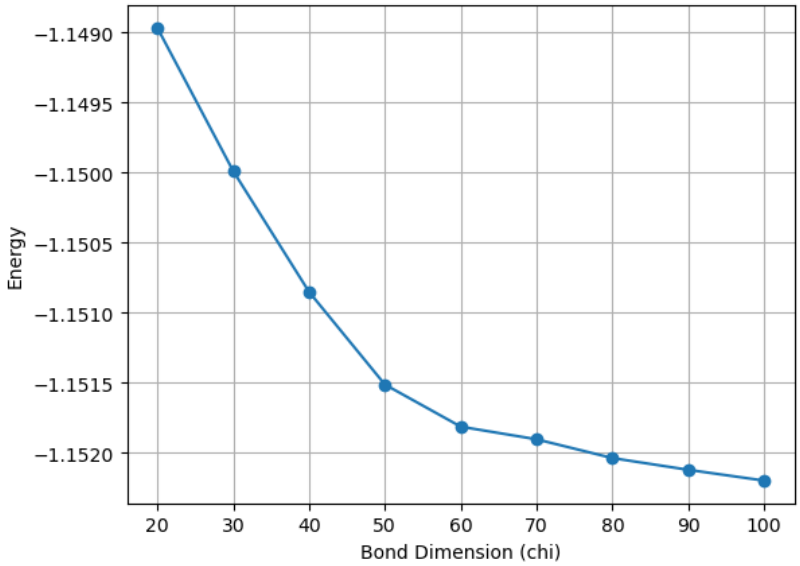

Figure 9: Plot showing how the ground state energy changes due to maximum bond dimension, chi.

4.2 Mean-field Theoretic Approach

Mean field theory (MFT) is a fundamental approach in physics that simplifies complex interacting systems by averaging the effects of all interactions. This technique is especially crucial in condensed matter systems because it reduces the complexity of the calculations needed to understand many-body systems.

High-temperature superconducting cuprate materials are typically layered, containing copper-oxide planes crucial to their superconducting properties, so they are complicated to solve numerically. The essential physics of the cuprates can be effectively modeled by lattice models like the Hubbard model on different types of lattices such as ladders. Cuprates are generally two/three-dimensional materials where the critical superconducting layers can be treated as two/three-dimensional planes. If we use mean field theory, we can derive an effective Hamiltonian to model cuprates in a lower dimension system which allows us to find analytic/numerical solutions more efficiently.

In our case, we concentrate on the 3D Hubbard model as seen in Fig. 10. We can host our general Hubbard model on 3D lattices as such $H = H_0 + t_\perp H_\perp$ with the inclusion of chemical potential and conserving particle number where [5]:

$$H_0 = \sum_{\langle R_i \rangle} H_0(R_i) = -t \sum_{R_i,\sigma} \sum_{n=1}^{L-1} \left(c^\dagger_{n+1,R_i,\sigma} c_{n,R_i,\sigma} + \text{H.c.} \right) - \mu \sum_{R_i,\sigma} \sum_{n=1}^{L} c^\dagger_{n,R_i,\sigma} c_{n,R_i,\sigma} + U \sum_{R_i} \sum_{n=1}^{L} n_{n,R_i,\uparrow} n_{n,R_i,\downarrow} \tag{44}$$

$$H_\perp = -\sum_{n} \sum_{\langle R_i \rangle} \sum_{\hat{a} \in \{\hat{y},\hat{z}\}} \left(c^\dagger_{n,R_i+\hat{a},\sigma} c_{n,R_i,\sigma} + \text{H.c.} \right) \tag{45}$$

We can start from this Hamiltonian and attempt to reduce its dimensionality to a quasi-one-dimensional model. We can begin by using second-order perturbation theory, and we can expand $H_\perp^2$ into

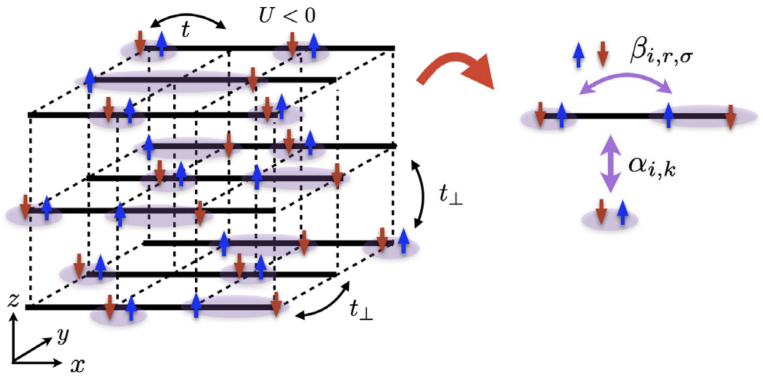

Figure 10: Diagram showing the 3-D ladder structure reducing to the quasi-1D chain [5].

$$H_\perp^2 = \sum_{n,m}\sum_{R_i,R_j}\sum_{\hat{a},\hat{b}\in\{\hat{y},\hat{z}\}}\sum_{\sigma,\sigma'}\Big(c^\dagger_{n,R_i+\hat{a},\sigma}c_{n,R_i,\sigma}c^\dagger_{m,R_j+\hat{b},\sigma'}c_{m,R_j,\sigma'}+c^\dagger_{n,R_i+\hat{a},\sigma}c_{n,R_i,\sigma}c^\dagger_{m,R_j,\sigma'}c_{m,R_j+\hat{b},\sigma'}+$$
$$c^\dagger_{n,R_i,\sigma}c_{n,R_i+\hat{a},\sigma}c^\dagger_{m,R_j+\hat{b},\sigma'}c_{m,R_j,\sigma'}+c^\dagger_{n,R_i,\sigma}c_{n,R_i+\hat{a},\sigma}c^\dagger_{m,R_j,\sigma'}c_{m,R_j+\hat{b},\sigma'}\Big)$$
$$= H_{\text{pair}} + H_{\text{exc}} \quad (46)$$

Where H_{pair} corresponds to pairs of fermions that jump from different chains to others, conserving spin but not the particle number per chain. The second operator H_{exc} corresponds to fermions switching switching chains (exchange). Thus, we now attempt to use the following ansatz to reduce our 3D Hamiltonian to a quasi-1D Hamiltonian and also assume that the expectation of operators that create/annihilate particles on different chains is 0:

$$\langle c_i c_j c_k c_l\rangle = \langle c_i c_j\rangle\langle c_k c_l\rangle + \langle c_i c_l\rangle\langle c_j c_k\rangle - \langle c_i c_k\rangle\langle c_j c_l\rangle \quad (47)$$

From this mean-field ansatz, we can now reduce each chain R_i of H_{pair} (assuming all chains are identical). Skipping steps that are fully derived in the appendix of [5], we arrive at the result where $z_c = 4$ is the coordination number:

$$H_{\text{pair,MF}} = -\sum_{n,m}\sum_{\hat{a}\in\{\hat{y},\hat{z}\}}\sum_{\sigma}\Bigg(\langle c^{\dagger}_{n,R_i+\hat{a},\sigma}c^{\dagger}_{m,R_i+\hat{a},-\sigma}\rangle c_{n,R_i,\sigma}c_{m,R_i,-\sigma} + c^{\dagger}_{n,R_i,\sigma}c^{\dagger}_{m,R_i,-\sigma}\langle c_{n,R_i+\hat{a},\sigma}c_{m,R_i+\hat{a},-\sigma}\rangle +$$
$$\langle c^{\dagger}_{n,R_i-\hat{a},\sigma}c^{\dagger}_{m,R_i-\hat{a},-\sigma}\rangle c_{n,R_i,\sigma}c_{m,R_i,-\sigma} + c^{\dagger}_{n,R_i,\sigma}c^{\dagger}_{m,R_i,-\sigma}\langle c_{n,R_i-\hat{a},\sigma}c_{m,R_i-\hat{a},-\sigma}\rangle\Bigg)$$
$$= 2z_c\sum_{n,m}\Big(\langle c_{n,\uparrow}c_{m,\downarrow}\rangle c_{n,\uparrow}c_{m,\downarrow} + \langle c_{n,\uparrow}c_{m,\downarrow}\rangle c^{\dagger}_{m,\downarrow}c^{\dagger}_{n,\uparrow}\Big) \quad (48)$$

Summarizing, we can condense our Hamiltonian into the following:

$$H_{\text{MF}} = H_0(R_i) - \sum_{i,k}\alpha_{i,k}(c_{i,\uparrow}c_{k,\downarrow} + c^{\dagger}_{k,\downarrow}c^{\dagger}_{i,\uparrow}) + \sum_{i,\sigma}\sum_{r=1}^{L-i}\beta_{i,r,\sigma}(c^{\dagger}_{i+r,\sigma}c_{i,\sigma} + c^{\dagger}_{i,\sigma}c_{i+r,\sigma}) \quad (49)$$

- Where we have the following coefficients describing tunneling in and out of parts of the 3D system [5]:
  - $\alpha_{i,k} = \frac{2z_c t_{\perp}^2}{\Delta E_p}\langle c_{i,\uparrow}c_{k,\downarrow}\rangle$
  - $\beta_{i,r,\sigma} = \frac{2z_c t_{\perp}^2}{\Delta E_p}\langle c^{\dagger}_{i+r,\sigma}c_{i,\sigma}\rangle$
- Each R_i denotes an individual chain.

Note the above derivation was very closely adapted from [5]. We can also see that $\alpha_{i,k}$ closely resembles the bound state pair wave function. From this effective mean-field Hamiltonian, we can now use a MPS algorithm to solve for our Hamiltonian.

4.3 MPS+MF Algorithm

We finally look at the following scheme in Fig. 11 detailing an iterative process to approximate our α and β values by solving the MPS using DMRG in order to approximate our effective quasi-one dimensional Hamiltonian.

- Note that we do not conserve particle number with our effective 1D Hamiltonian although this was the case in our explicit 3D Hamiltonian.
- Our scheme largely depends on initial guesses of coefficients and also scales with bond dimension as well as system size (due to DMRG).

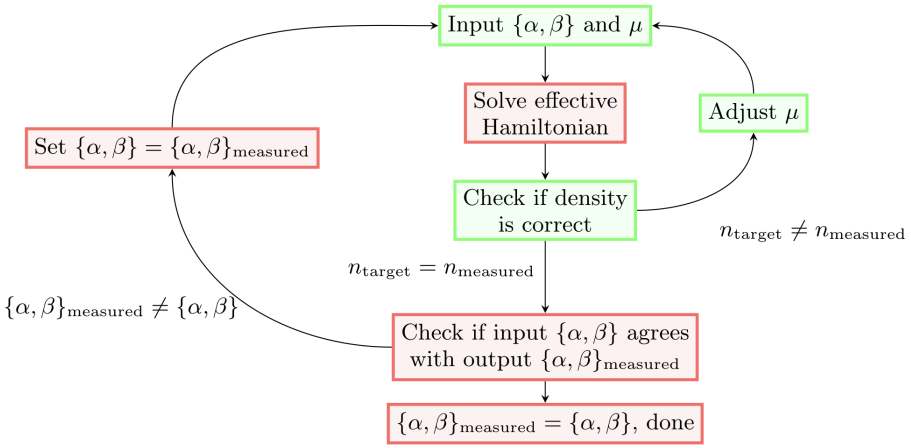

Figure 11: A schematic diagram of the MPS+MF convergence process [5]

Specifically in this algorithm, we choose to use DMRG to solve our effective Hamiltonian although any MPS method may be used and the only requirement is that the mean-field amplitudes converge [5]. Also, because of the existence of a spin gap, we are guaranteed that α and β decay exponentially with distance making numerical schemes much easier to use. Although we have not explored this algorithm to its fullest extent, we plan to use it in the future to understand different lattice systems apart from higher dimensional ladder structures in order to help numerically understand cuprate/high-temperature superconductivity.

4.4 Conclusion and Future Outlook

In this thesis, we discussed the basics of the Hubbard model and its extensions to deepen our understanding of superconductivity in cuprate materials. Specifically, we explored the t-J model, Heisenberg model, and attractive-U Hubbard phase. In doing so, we also discussed important theoretical approaches and methods such as the Holstein-Primakoff transformation, BCS theory, and the Meissner effect. In addition, we gave a brief introduction to matrix product states and DMRG. Through rigorous computational analyses utilizing these tensor network methods, we have found that the attractive 1-D Hubbard model has signatures of superconductivity and have also compared theoretical approaches to approximating the 1-D Hubbard ground state from the literature with our numerical simulations.

As we look to the future, the integration of mean-field approaches with tensor

network states as described by [5] holds promising potential for tackling the challenges of two/three-dimensional cuprate systems and exploring high-Tc superconductors in general. We seek to determine the mean-field/DMRG method's validity for use in broader applications such as more complicated lattice structures such as two-dimensional triangular lattices and also seek to make improvements to the MPS+MF method with respect to convergence times. Furthermore, we look to include other ways to investigate high-temperature superconductivity such as including next-nearest neighbor hopping in the 2D Hubbard model, and hope to push the limit of observing superconducting phases by perturbing the Hubbard model.

Through this thesis, we have given a review of the basics of models of superconductivity as well as numerical methods useful in understanding high-temperature superconductivity and the critical role of electron correlations. This work not only reinforces the Hubbard model's foundational relevance but also enhances our computational toolkit for probing the quantum landscape of superconducting materials, providing a stepping stone for future projects in the field.

References

[1] Density matrix renormalization group (dmrg). `https://tensornetwork.org/mps/algorithms/dmrg/`. Accessed: 2024-05-09.

[2] Daniel P. Arovas, Erez Berg, Steven A. Kivelson, and Srinivas Raghu. The hubbard model. *Annual Review of Condensed Matter Physics*, 13:239–274, 2022.

[3] Assa Auerbach. *Interacting Electrons and Quantum Magnetism*. Springer-Verlag, New York, 1994.

[4] J. Bardeen, L. N. Cooper, and J. R. Schrieffer. Theory of superconductivity. *Phys. Rev.*, 108:1175–1204, Dec 1957.

[5] Gunnar Bollmark, Thomas Köhler, Lorenzo Pizzino, Yiqi Yang, Johannes S. Hofmann, Hao Shi, Shiwei Zhang, Thierry Giamarchi, and Adrian Kantian. Solving 2d and 3d lattice models of correlated fermions—combining matrix product states with mean-field theory. *Phys. Rev. X*, 13:011039, Mar 2023.

[6] Fabian H. L. Essler, Holger Frahm, Frank Göhmann, Andreas Klümper, and Vladimir E. Korepin. *The One-Dimensional Hubbard Model*. Cambridge University Press, 2005.

[7] Susumu Yamada et al. High performance lobpcg method for solving multiple eigenvalues of hubbard model: Efficiency of communication avoiding neumann expansion preconditioner. pages 243–256, 2018.

[8] Matthew B. Hastings and Tohru Koma. Spectral gap and exponential decay of correlations. *Communications in Mathematical Physics*, 265(3):781–804, April 2006.

[9] Johannes Hauschild and Frank Pollmann. Efficient numerical simulations with Tensor Networks: Tensor Network Python (TeNPy). *SciPost Phys. Lect. Notes*, page 5, 2018. Code available from `https://github.com/tenpy/tenpy`.

[10] Hong-Chen Jiang and Steven A. Kivelson. Stripe order enhanced superconductivity in the hubbard model. *Proceedings of the National Academy of Sciences*, 119(1):e2109406119, 2022.

[11] Elliott H. Lieb and F. Y. Wu. Absence of mott transition in an exact solution of the short-range, one-band model in one dimension. *Phys. Rev. Lett.*, 20:1445–1448, Jun 1968.

[12] Román Orús. A practical introduction to tensor networks: Matrix product states and projected entangled pair states. *Annals of Physics*, 349:117–158, October 2014.

[13] G. Polatsek and K. W. Becker. Ground-state energy of the hubbard model at half filling. *Phys. Rev. B*, 54:1637–1644, Jul 1996.

[14] Mingpu Qin, Thomas Schäfer, Sabine Andergassen, Philippe Corboz, and Emanuel Gull. The Hubbard model: A computational perspective. *Annual Review of Condensed Matter Physics*, 13(1):275–302, March 2022.

[15] P B Ramos and M J Martins. Algebraic bethe ansatz approach for the one-dimensional hubbard model. *Journal of Physics A: Mathematical and General*, 30(7):L195, apr 1997.

[16] Sachdev S. *Quantum Phase Transitions*. Cambridge university press, 1998.

[17] R. T. Scalettar, E. Y. Loh, J. E. Gubernatis, A. Moreo, S. R. White, D. J. Scalapino, R. L. Sugar, and E. Dagotto. Phase diagram of the two-dimensional negative-u hubbard model. *Phys. Rev. Lett.*, 62:1407–1410, Mar 1989.

[18] U. Schollwöck. The density-matrix renormalization group. *Rev. Mod. Phys.*, 77:259–315, Apr 2005.

[19] B. Sriram Shastry. Mott transition in the hubbard model. *Modern Physics Letters B*, 06(23):1427–1438, 1992.

[20] Luca F. Tocchio, Federico Becca, and Sandro Sorella. Hidden mott transition and large-u superconductivity in the two-dimensional hubbard model. *Phys. Rev. B*, 94:195126, Nov 2016.

[21] Hao Xu, Chia-Min Chung, Mingpu Qin, Ulrich Schollwöck, Steven R. White, and Shiwei Zhang. Coexistence of superconductivity with partially filled stripes in the Hubbard model, March 2023. arXiv:2303.08376 [cond-mat, physics:physics].